

Effect of Magnetic Field Profile on the Anode Fall in a Hall Thruster

IEPC-2005-002

Presented at the 29th International Electric Propulsion Conference, Princeton University,
October 31 – November 4, 2005

Leonid A. Dorf*, Yevgeny F. Raitses, and Nathaniel J. Fisch
Princeton Plasma Physics Laboratory (PPPL), Princeton, NJ, 08543, USA

Effect of the magnetic field profile on the anode fall in a 2 kW laboratory Hall thruster is studied both experimentally and theoretically. Plasma potential, electron temperature, and plasma density in the near-anode region are measured with a biased probe in three configurations of the magnetic field. It is observed that the anode fall in a Hall thruster can be changed from negative to positive by creating a magnetic field configuration with a zero magnetic field region. Similar configurations are utilized in some advanced Hall thrusters. Results of the measurements are employed to model a Hall thruster with different magnetic field configurations, including the one with a zero-field region. Different anode sheath regimes observed experimentally are used to set the boundary conditions for the quasineutral plasma. Numerical solutions obtained with a hydrodynamic quasi-1D model suggest that varying the magnetic configuration affects the electron mobility both inside and outside the channel, as well as the plasma density distribution along the axis. Different mobilities inside and outside the channel have been discussed in recent theoretical works in conjunction with modeling of the conventional (like SPT-100) and advanced (like ATON) thrusters.

I. Introduction

A plasma thruster with closed electron drift, or so-called Hall thruster (HT), is currently one of the most advanced and efficient types of electrostatic propulsion devices.^{1,2} The principle of operation of Hall thrusters is based on electrostatic acceleration of heavy ions in crossed electric and magnetic fields applied to a dc plasma discharge. Conventional Hall thrusters have a coaxial structure, and consist of electromagnetic coils with a ferromagnetic core, an anode that also serves as a gas distributor, a ceramic channel, and a cathode-neutralizer (Fig. 1). The electric field is induced in a quasineutral plasma by an applied dc voltage, V_d , typically of the order of several hundred volts. An applied radial magnetic field (with a maximum strength of typically between a hundred and two hundred Gauss) in the presence of the axial electric field causes the magnetized electrons to drift in the azimuthal direction – this drift is called a Hall drift. The axial flow of electrons toward the anode is therefore impeded, providing sufficient electron residence time for effective ionization at a discharge current, I_d , that does not greatly exceed a total outgoing ion current, I_i . The ratio I_i/I_d is the definition of current utilization – one of the important factors determining thruster efficiency. Another advantage of employing a magnetic field in Hall thrusters is that, due to the decreased electron mobility, the main discharge voltage drop occurs in the plasma, and not in the non-neutral sheath near the cathode like in regular glow and arc discharges. Thus, the acceleration of unmagnetized ions by the electric field occurs in the quasineutral plasma, and is not limited by space-charge effects that are present, for example, in electrostatic-grid ion thrusters.³⁻⁵ Experimental and theoretical studies of the effect of the radial magnetic field axial profile on Hall thruster operation concluded that plasma flow is more stable in regions where the magnetic field increases in the direction of ion flow, and more unstable (with respect to formation of an azimuthally rotating “spike” that perturbs uniformity of the discharge) in regions where magnetic field decreases.⁶⁻⁸ Therefore, the magnetic field profile employed in conventional Hall thrusters generally satisfies the plasma flow stability criterion, $dB_r(z)/dz > 0$, along most of the thruster channel.

* Present address: Los Alamos National Laboratory, Los Alamos, NM 87545; e-mail address: ldorf@lanl.gov.

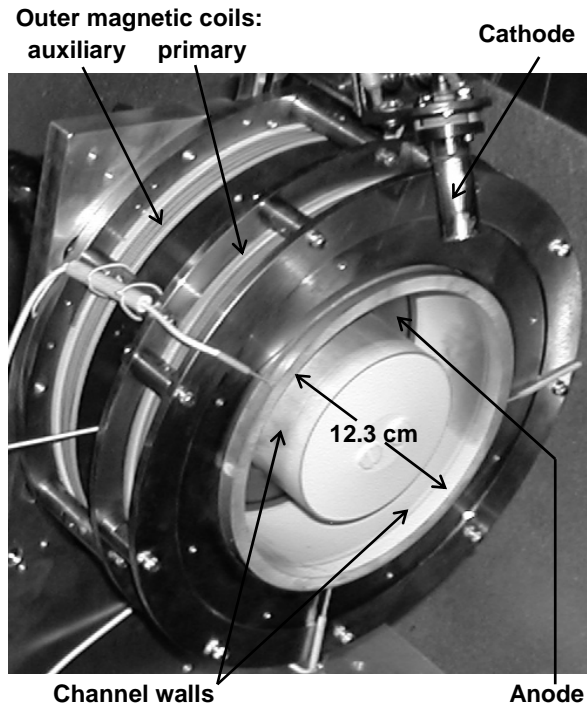


Figure 1. The 2 kW laboratory Hall thruster with 12.3 cm outer channel wall diameter.

measurements of the plasma potential allowed the first experimental identification of both electron-repelling (negative anode fall) and electron-attracting (positive anode fall) anode sheaths in a HT. It was shown that at typical thruster operating conditions the fall at the clean anode is negative, which is in agreement with the results of a recent theoretical study of the anode sheath in HTs.^{25,26,28} At typical operating conditions, the thermal electron current to the anode, produced by ionization in the quasineutral plasma, is larger than the discharge current. Therefore, the formation of a negative fall is required to repel the excessive electron flux from the anode.²⁶ Such anode fall behavior, essentially opposite to that in glow discharges, is the result of a very high ionization degree in HTs achieved by applying a radial magnetic field transverse to the direction of the discharge current.

Similar to Hall thrusters, a magnetic field transverse to the direction of the discharge current is also utilized in other gas discharge devices, such as magnetrons and magneto-plasma-dynamic thrusters. The effect of the magnetic field on anode and cathode falls in these devices and in regular dc-glow discharges was studied both experimentally and theoretically.²⁹⁻³⁴ The use of the transverse magnetic field in glow discharges was generally shown to result in a decrease of the cathode potential drop and an increase of the anode potential drop, which was attributed to a reduced electron mobility.^{31,32,34} Whereas in these works the magnetic field was typically homogeneous throughout the entire discharge, in conventional Hall thrusters the magnetic field is significant only in the so-called acceleration region, which starts about half of the channel length from the anode and where the main voltage drop occurs. Therefore, to study the effect of the magnetic field on the anode fall in Hall thrusters, a special magnetic field configuration with a non-zero field near the anode needs to be created.

In this paper we present results of plasma measurements in the near-anode region of the 2 kW laboratory Hall thruster with three different configurations of the magnetic field, performed with a biased probe. Literature search suggests that this is the first experimental study of the effect of the magnetic field profile on the anode fall in Hall thrusters. It is observed experimentally that an anode fall in a Hall thruster can be changed from negative to positive by using a special magnetic field that changes polarity somewhere along the channel. Measured plasma potential, electron temperature, and plasma density are employed here to model a Hall thruster with different magnetic field configurations. Numerical solutions obtained with a hydrodynamic quasi-1D model suggest that varying the magnetic field configuration can affect the electron mobility both inside and outside the channel, as well as the plasma density distribution along the thruster axis.

In a gas discharge, there can be either an increase or a drop in the plasma potential over a distance of a few Debye lengths from the anode, generally referred to in the literature as the “anode fall”. When the anode is at a higher potential than the near-anode plasma, the anode fall is called “positive”, and when it is at a lower potential – “negative”. The positive and negative anode falls are associated with formation of the electron-attracting and electron-repelling anode sheaths, respectively. In spite of a number of experimental⁹⁻²⁰ and theoretical²¹⁻²⁴ studies of a Hall thruster internal plasma structure, the understanding of the anode sheath phenomena in Hall thrusters was, until recently, very limited. A more detailed review of previous works and additional motivation for studying the anode sheath phenomena in Hall thrusters can be found in Refs. 25 and 26. As was reported recently, a diagnostic apparatus comprising biased and emissive electrostatic probes, a high-precision positioning system, and low-noise electronic circuitry was developed and used for measurements in the near-anode region of the 12.3 cm Hall thruster operating in the 0.2 – 2 kW power range^{25,27}. Accurate, non-disturbing

The paper is organized as follows. In Section II, we describe the 12.3 cm Hall thruster with three different magnetic field configurations and the biased electrostatic probe apparatus used in this study. In Sections III and IV, we discuss the results of plasma measurements, and examine the effect of the magnetic field on the anode fall. In Section V we introduce the hydrodynamic quasi-1D model describing a quasineutral plasma in a Hall thruster. We conclude in Section VI with analysis of the numerical results.

II. Experimental Procedure

The test facility, the 2 kW laboratory Hall thruster, and the electrostatic probe apparatus used in this study are described in detail in Refs. 35 and 27. The thruster has a conventional annular configuration with a channel length $L_{ch} = 46\text{ mm}$ (which is in the 20 – 80 mm range typical for HTs)⁹⁻²⁰, a channel width $H_{ch} = 25\text{ mm}$, and an outer channel wall diameter $D_{out} = 12.3\text{ cm}$ (Fig. 1). In the present experiments, the thruster was operated at xenon gas mass flow rate $\dot{m} = 3\text{ mg/s}$, and at the discharge voltage $V_d = 300\text{ V}$. The anode surface facing the plasma was thoroughly cleaned before the experiments to ensure its conductivity.²⁵

The magnetic field in the thruster was created by one inner and two outer, primary and auxiliary, electromagnetic coils (Fig. 1). The currents in the inner and primary outer coils were kept equal to 1.3 A throughout the experiments, whereas different currents, $I_c = 0$, $I_c = 1.4\text{ A}$, and $I_c = -1.4\text{ A}$, were supplied to the auxiliary outer coil to create three configurations of the magnetic field, B_0 , B_{pos} , and B_{neg} , respectively. Figs. 2 and 3 show results of non-linear simulations of the magnetic field distribution. Simulations were conducted using measured B-H curve of the low carbon steel used in the thruster design. A comparison of simulated and measured results showed a very good agreement.

The plasma potential, plasma density and electron temperature were measured at 2, 7 and 12 mm from the anode with a movable biased electrostatic probe of planar geometry. The anode sheath thickness, typically assumed to be several Debye lengths, $\lambda_D \sim 0.05\text{--}0.2\text{ mm}$, is very small in the near-anode region of a Hall thruster, which makes technically difficult the use of probe diagnostics inside the sheath. However, information about the sign and magnitude of the anode fall can be obtained through probing plasma in the presheath, at a few millimeters from the anode. The probe was introduced radially into the near-anode region through the axial slot made in the outer channel wall. As was reported in Ref. 27, the motion of the radially-oriented probe near the anode does

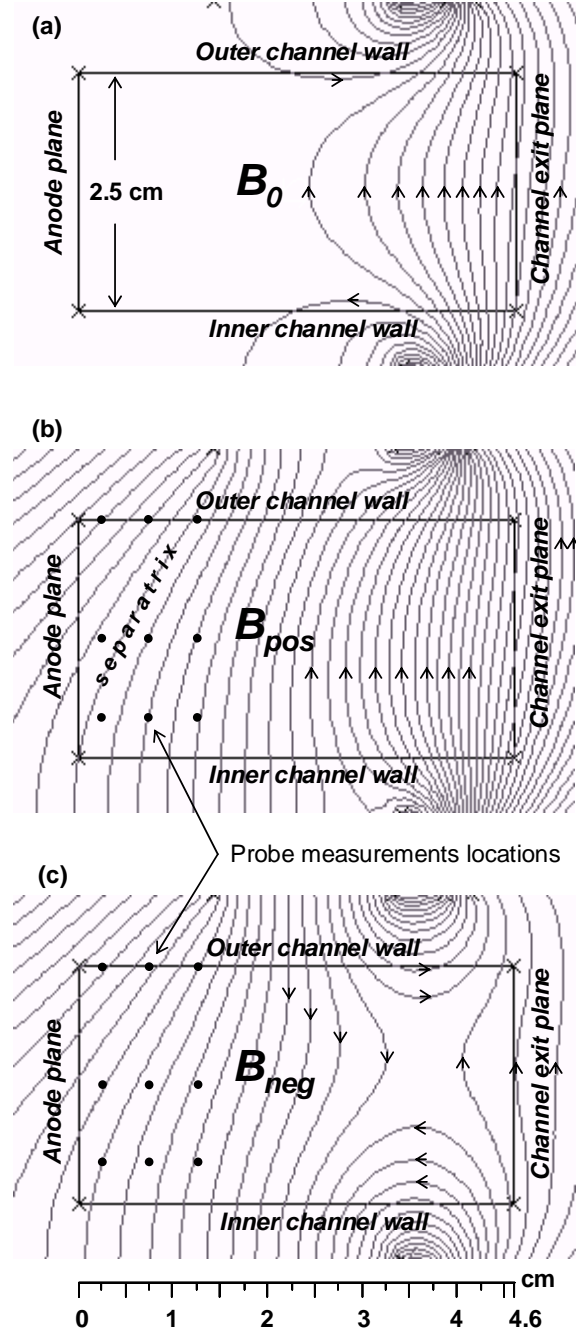


Figure 2: Magnetic field lines in the 12.3 cm Hall thruster for three magnetic field configurations, B_0 , B_{pos} , and B_{neg} . All diagrams are drawn to scale.

not cause perturbations to the Hall thruster discharge. The plasma measurements were performed at several distances from the thruster axis: at the outer wall (OW), $R = 62$ mm, in the mid-point between the channel walls (MC), $R = 49$ mm, and near the inner wall (IW), $R = 41$ mm, as shown in Fig. 2.

The biased planar probe was constructed of 0.76 mm diameter thoriated tungsten rod, covered by a high purity alumina single bore tube with outer diameter of 1.3 mm and inner diameter of 0.79mm. The planar tip geometry was chosen because, in the near-anode region, the voltage-current characteristics of a planar probe appear to have more distinctive electron and ion saturation than those of a cylindrical probe.²⁷ For the unmagnetized probe theory to be valid for a cylindrical probe introduced into plasma perpendicular to the magnetic field lines, the probe diameter must be much smaller than the electron gyrodiameter.³⁶ A similar criterion for a planar probe introduced into plasma at an angle to the magnetic field can be formulated as that the collecting rod diameter, d , projected onto the magnetic field line must be much smaller than the electron gyrodiameter. When the planar probe is introduced radially into the thruster channel, this criterion can be expressed as $d \ll 4.8\sqrt{T_e(\text{eV})} / B_z(\text{G})$, where B_z is the

axial component of the magnetic field. In this study, the most severe limitation is imposed in B_{neg} configuration for measurements at the outer wall and at 7 mm from the anode: $d_{pr} \ll 2$ mm. For the collecting rod diameter employed, $d = 0.76$ mm, this limitation is marginally satisfied.

The probe was biased relative to the anode with a bipolar power supply, which was programmed with a one cycle sinusoidal signal by a PC-based function-generator connected through an isolation amplifier. A 500 Ω shunt was used for measurements of the electron part of the probe current-voltage characteristic. The probe current and biasing voltage were measured through isolation amplifiers, because anode and probe potentials to ground were about 300 V in these measurements. The data and error analysis procedures for biased probe measurements are described in detail in Ref. 27.

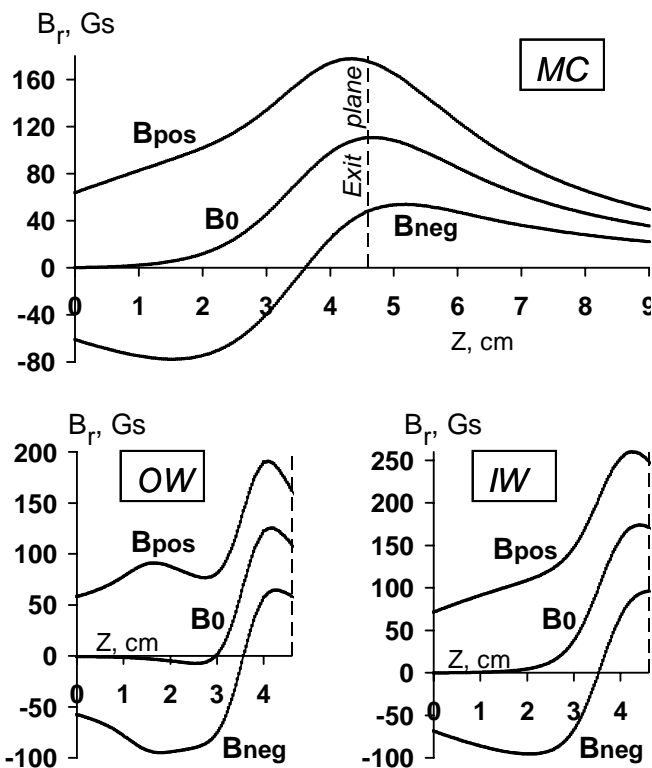


Figure 3: Radial magnetic field axial profiles, $B_r(z)$, in the 12.3 cm Hall thruster for three magnetic field configurations, B_0 , B_{pos} and B_{neg} . $Z = 0$ is chosen at the anode. (a) – at the mid point between the channel walls (MC); (b) – at the outer wall (OW); (c) – at 4 mm from the inner wall (IW).

III. Experimental Results

Fig. 4 shows plasma potential axial profiles, $\Phi_{pl}(z)$, measured in the near-anode region of the 12.3 cm Hall thruster with three magnetic field configurations, B_0 , B_{pos} , and B_{neg} , along with the measured discharge current, I_d . At each of the nine locations inside the channel, measurements were performed sequentially in all three configurations of the magnetic field. The error bars for Φ_{pl} measured at the outer wall and at 2 mm from the anode in B_{neg} configuration are not shown in the Fig. 4 (c). A kink in the probe current-voltage characteristic, I_{PR} vs. V_{PR} , normally used to determine plasma potential,²⁷ was hard to distinguish for this data point due to the lack of plasma at the described location inside the channel. Instead, the kink in the $\ln(I_{PR})$ vs. V_{PR} plot was used, and the uncertainty in determining Φ_{pl} by this method is hard to estimate.

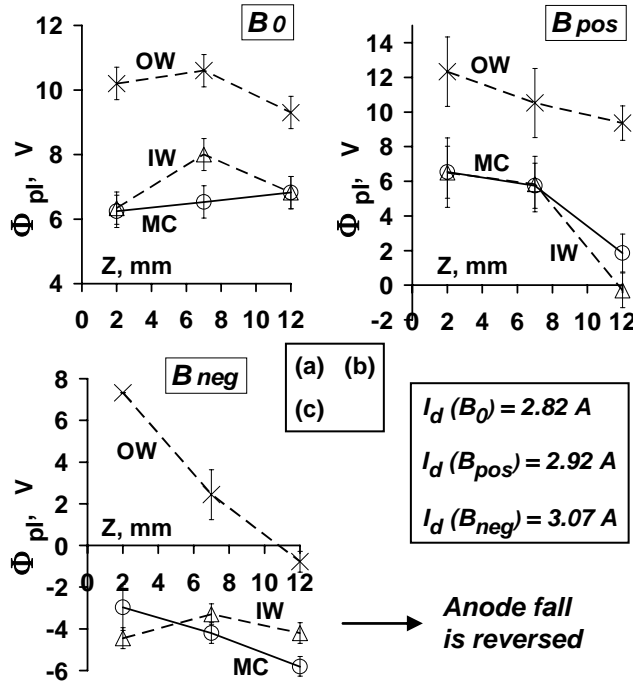


Figure 4: Plasma potential axial profiles, $\Phi_{pl}(z)$, for three magnetic field configurations, B_0 , B_{pos} , and B_{neg} , measured with the biased probe at several radial locations – at the outer wall (OW), at the mid point between channel walls (MC), and at 4 mm from the inner wall (IW) – in the near-anode region of the 12.3 cm Hall thruster at $V_d = 300$ V and $\dot{m} = 3$ mg/s. $Z=0$ is chosen at the anode, and Φ_{pl} is shown relative to the anode potential. Also shown are measured discharge currents, I_d .

channel median, as follows from measurements of the plasma density axial profiles, $N(z)$, at three radial locations, IW, MC, and OW [Figs. 5 (b) and (c)]. Furthermore, the plasma density near the inner wall and near the channel median at 2 mm from the anode is almost the same in these configurations as it is in B_0 configuration, in which the near-anode magnetic field is negligible [Fig. 2 (a)]. Interestingly, measurements at 2.5 mm from the anode in a discharge similar to the Hall thruster discharge showed that the near-anode plasma density increases with the increase of the magnetic field.²⁹ However, in Ref. 29, the magnetic field was uniform throughout the entire discharge, and it was strictly parallel to the anode surface, unlike the near-anode magnetic field in B_{neg} and B_{pos} configurations in the present study [Figs. 2 (b) and (c)].

In B_{pos} and B_{neg} configurations, the radial magnetic field in the near-anode region is comparable to that in the acceleration region (Fig. 3). The radial magnetic field impedes the electron motion toward the anode. In B_{pos} configuration, the electron transport across the magnetic field is provided by the negative axial gradient of the plasma potential and the positive axial gradient of the electron pressure, observed at the IW and MC radial locations [Figs. 4 (b) and 5 (b)]. In B_{neg} configuration, the electron transport across the magnetic field is governed mainly by the axial electron pressure gradient, $\frac{1}{eN} \frac{dP}{dz} \sim 8$ V/cm, since it is

larger than the gradient of the plasma potential near the inner wall and at the channel median [Figs. 4 (c) and 5 (c)]. In the near-anode region, the ion velocity is much less than the electron velocity and the electron temperature is almost constant along the channel [Figs. 5 (e) and (f)]. Therefore, at 7 – 12 mm from the anode in B_{pos} and B_{neg} configurations, the phenomenological electron momentum equation describing the electron axial transport across the magnetic field²⁸ can be written as

As can be seen from Fig. 4 (a), the plasma potential at 2 mm from the anode is higher than the anode potential in all three radial locations, IW, MC, and OW, which indicates the presence of a negative anode fall, or electron-repelling anode sheath, in a conventional Hall thruster with B_0 configuration of the magnetic field. In the quasineutral plasma between the anode and the acceleration region, the electron drift velocity, $V_{dr} \sim I_d / (e \cdot N_0 \cdot AA) \approx 6 \cdot 10^6$ cm/s, is much smaller than the average velocity of the half-Maxwellian electron flux traveling towards the anode, $V_{HM} = \sqrt{2T_e / (\pi m_e)} \approx 8 \cdot 10^7$ cm/s, as can be estimated using the channel cross-section, $AA = 77$ cm², the measured discharged current, $I_d = 2.82$ A, and the plasma density, N_0 , along with the electron temperature, T_e , measured in the mid-point between the channel walls at 2 mm from the anode [Figs. 5 (a) and (d)]. At the mass flow rates typical for the HTs, electron-neutral collisions are very weak near the anode ($\Lambda_{en} \sim \Lambda_{mn} \approx 10 - 20$ cm), so is the magnetic field in the conventional HT configuration [Fig. 3 (a)]. Therefore, to create a reversed electron flux and reduce the net electron velocity, formation of the electron-repelling anode sheath is required in B_0 configuration.

In B_{pos} and B_{neg} configurations, most of the plasma in the near-anode region is concentrated between the inner wall and the

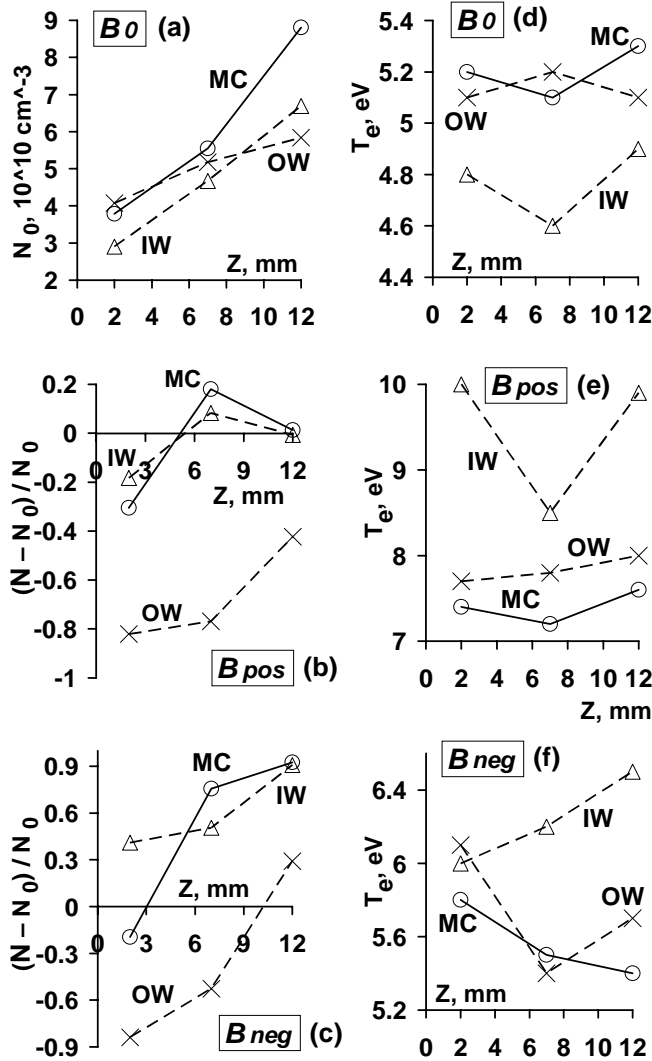


Figure 5: (a) – plasma density axial profiles, $N_0(z)$, for B_0 configuration, (b) – (c) – relative density profiles, $[N(z) - N_0(z)]/N_0(z)$, for B_{pos} and B_{neg} configurations, and (d) – (f) – electron temperature profiles, $T_e(z)$, for all three configurations. Measured with the biased probe at several radial locations – at the outer wall (OW), at the mid point between channel walls (MC), and at 4 mm from the inner wall (IW) – in the near-anode region of the 12.3 cm Hall thruster at the discharge voltage $V_d = 300$ V and the mass flow rate $\dot{m} = 3$ mg/s. $Z = 0$ is chosen at the anode.

because of the presence of a shear plasma flow with periodically changing azimuthal velocity, created by the periodic $\mathbf{J} \times \mathbf{B}$ force. In summary, transport-inducing instabilities might be reduced in a HT by the presence of the zero magnetic field region. In light of the above, one intuitively appealing argument is that the reversal of polarity of the anode fall in B_{neg} configuration [Fig. 4 (c)] could be attributed to the reduced mobility inside the channel.

$$J_d \approx \mu_e [(T_e/e) \cdot dN/dz - N \cdot d\Phi_{pl}/dz]$$

where $J_d = I_d/(e \cdot AA)$, e is the absolute value of the electron charge, and μ_e is the electron axial mobility in a radial magnetic field. Using the measured plasma potential, plasma density, and electron temperature (Figs. 4 and 5), and assuming that at 7 – 12 mm from the anode, N and Φ_{pl} are linear functions of z , the value of the electron axial mobility in the near-anode region in B_{pos} and B_{neg} configurations can be estimated as

$$\mu_e \sim (1/7 - 1/4) \cdot |B_r|^{-1} \sim (20 - 30) \text{ T}^{-1},$$

which is greater than the Bohm value, $\mu_e = 1/16 \cdot |B_r|^{-1}$. Note that for the low-power cylindrical Hall thruster (CHT), which has a cusp magnetic field configuration similar to B_{neg} , the value of the electron axial mobility that gives the best agreement between the simulations and experiments was found to be close to the Bohm value.³⁷ The same is true for the value of the electron mobility obtained experimentally in Hall thrusters¹⁹, whereas the value of the axial mobility typically used in theoretical models is significantly smaller than the Bohm value.^{21,28,38}

Note also that the anomalous electron transport in HTs is believed to be induced by high-frequency plasma instabilities. Interestingly, in the frequency range below ~ 100 kHz, the 2.6 cm CHT with the cusp magnetic field operates quieter than the annular Hall thruster of the same size.³⁹ The theoretical study of a HT, reported in Ref. 40, also shows that the amplitude of the low frequency current oscillations (10 – 20 kHz) decreases, when the B field configuration exhibits a zero field inside the channel. This improved stability has been observed experimentally in the ATON Hall thruster, where the magnetic field topology includes a point of zero- B field.⁴⁰⁻⁴² Finally, in Ref. 43, the stabilization of a longitudinal dc discharge is achieved by applying a spatially periodic radial external magnetic field which varies in sign along the axis of the coaxial system. The uniformity of the discharge improves

IV. Anode Fall in B_{pos} and B_{neg} Configurations

As can be seen from Figs. 2 (b) and (c), electrons that are transferred sufficiently close to the anode can reach the anode along the magnetic field lines. In Fig. 2 (b), the magnetic field line that separates the electrons bouncing between the channel walls from the electrons escaping to the anode is labeled “separatrix”. Electron thermal motion toward the anode along the magnetic field lines is not impeded by the magnetic field. Moreover, bulk of the electrons transferred onto the magnetic field lines connected to the anode with longitudinal velocities directed toward the outer wall are repelled by the wall sheath, and eventually also reach the anode (Fig. 2). Therefore, it can be assumed that in B_{pos} and B_{neg} configurations, the potential drop between the near-anode plasma and the anode is again required to repel the excessive electron flux from the anode. This could explain the presence of the negative anode fall observed at IW and MC radial locations in B_{pos} configuration of the magnetic field [Fig. 4 (b)]. The structure of this sheath is not significantly affected by the magnetic field, because near the anode, the Larmor radius, $\rho_L = 2.4 \sqrt{T_e(\text{eV})} / B(\text{G}) \sim 0.8 \text{ mm}$, is 6 – 8 times greater than the Debye length, as can be estimated using the electron temperature and the plasma density measured at 2 mm from the anode near the inner wall and at the midpoint between the channel walls.

The following estimation can illustrate the physical picture described above. Assume: (a) – that at 2 mm from the anode, only electrons repelled by the voltage drop in the anode sheath, Φ_{pl} , have longitudinal velocities directed toward the outer wall, and (b) – that velocity distribution for electrons with longitudinal velocities directed toward the anode is half-Maxwellian. In this case, the total electron current toward the anode through the plane crossing the channel at 2 mm from the anode can be estimated as

$$I_e = e \cdot N \cdot V_{\parallel}^e \cdot \cos \alpha \cdot A_{\text{eff}}, \quad (4.1)$$

where
$$V_{\parallel}^e = \sqrt{2/\pi \cdot T_e/m_e} \times \exp(-e\Phi_{pl}/T_e) / (1 + \text{erf}(\sqrt{e\Phi_{pl}/T_e})) \quad (4.2)$$

and
$$A_{\text{eff}} = \beta \cdot AA. \quad (4.3)$$

In eq-s (4.1) and (4.2), all plasma properties are obtained by averaging between the values measured at IW and MC radial locations at 2 mm from the anode; $\alpha \approx 60^\circ$ is the angle between the magnetic field lines and the thruster axis; and $(\beta \cdot AA)$ is the effective cross-sectional area of the channel, which takes into account that not all magnetic field lines in the considered cross-section intersect with the anode [Figs. 2 (b) and (c)], and that the plasma density measured at the outer wall is much smaller than that measured in the midpoint between the walls or near the inner wall. Using the plasma potential, plasma density, and electron temperature measured in B_{pos} configuration at 2 mm from the anode [Figs. 4 (b), 5 (b), and 5 (e)], the electron current toward the anode in this magnetic configuration can be evaluated as $I_e \approx \beta_{\text{pos}} \cdot 4.5 \text{ A}$. Considering that at 2 mm from the anode the ion current constitutes a negligible part of the discharge current, $I_d = 2.92 \text{ A}$, the numerical factor β in B_{pos} configuration can be then estimated as

$$\beta_{\text{pos}} \approx I_d / 4.5 \approx 0.65. \quad (4.4)$$

In B_{neg} configuration, the plasma potential measured at 2 mm from the anode near the inner wall and at the channel median is lower than the anode potential [Fig. 4 (c)], which indicates the presence of a positive anode fall. Electrons traveling toward anode along the magnetic field lines are therefore not repelled by the voltage drop between the anode and the near-anode plasma. Using eq. (1) with $\Phi_{pl} = 0$ and plasma density, N , measured in B_{neg} configuration at 2 mm from the anode [Fig. 5 (c)], it can be obtained that $I_e = \beta_{\text{neg}} \cdot \sqrt{T_{\parallel}(\text{eV})} \cdot 6.25 \text{ A}$, where T_{\parallel} is the temperature associated with the electron motion along magnetic field lines. Assuming that $\beta_{\text{neg}} = \beta_{\text{pos}} = 0.65$, and using the value of the discharge current measured in B_{neg} configuration, $I_d = 3.07 \text{ A}$, it can be obtained that the parallel temperature should be equal to $T_{\parallel} \approx 0.6 \text{ eV}$. The electron temperature measured in B_{neg} configuration at all three radial locations at 2 mm from the anode is about 6 eV [Fig. 5 (f)]. The electron temperature measured by a planar probe in the bi-Maxwellian plasma in the magnetic field is $T_e = T_{\parallel} \sin^2 \alpha + T_{\perp} \cos^2 \alpha$, where T_{\perp} is the temperature associated with electron Larmor gyration, and α is the angle between the magnetic field and the collecting plane of the probe (for a radially inserted probe, α is the same as the angle between the magnetic field and the thruster axis). Thus, for $T_{\parallel} \approx 0.6 \text{ eV}$, it can be obtained that $T_{\perp} \approx 24 \text{ eV} \approx 40 \cdot T_{\parallel}$. Physical mechanisms

that could account for such strong anisotropy in the near-anode electron temperature are not apparent. Alternatively, it could be assumed that in B_{neg} configuration, the numerical factor β is different from that in B_{pos} configuration. For the isotropic electron temperature, $T_{\parallel} = T_{\perp} = T_e = 6\text{eV}$, it can be obtained that in B_{neg} configuration $\beta_{neg} = 0.2$, which is about three times less than that in B_{pos} configuration. Deeper understanding of such intricate phenomenon as the presence of a positive anode fall in B_{neg} configuration has yet to be obtained.

V. Theoretical Model

General issues associated with modeling of Hall thrusters are described in detail in Refs. 24 and 28. In this section, the quasi-1D model with a given temperature profile introduced in Ref. 24, along with the results of measurements in the near-anode region presented in Sec. III, are employed to describe the behavior of the quasineutral plasma in the 12.3 cm Hall thruster with three different configurations of the magnetic field (Fig. 2).

Using the experimentally obtained discharge current and near-anode plasma density along with a given temperature profile allows theoretical evaluation of certain plasma properties, like the electron axial mobility, which are hard to characterize experimentally. Unlike in Ref. 28, non-quasineutral plasma in the anode sheath is not considered here; instead, different anode sheath regimes observed experimentally are used to set the boundary conditions for the quasineutral plasma. Consequently, the voltage drop in the anode sheath is neglected, and the entire discharge voltage, $V_d = 300\text{V}$, is applied here to the quasineutral plasma. To make use of the experimental results, the propellant (Xenon) mass flow rate of $\dot{m} = 3\text{mg/s}$ and the radial magnetic field axial profiles given in the Fig. 3 (a) are used in the numerical simulations.

Incorporating the electron energy balance equation into the full system of equations proved to be a rather difficult task in conventional HTs, due in part to a non-Maxwellian shape of the electron distribution function, which was observed in HTs.^{44,45} In a HT with a non-conventional magnetic field configuration this task becomes even more complicated, due to the presence of a significant axial component of the magnetic field. The axial magnetic field impedes electron motion toward the channel walls, which could reduce the electron energy losses in that region. Therefore, due to the lack of the experimentally obtained temperature profiles in B_{pos} and B_{neg} configurations, simplified profiles were used here in modeling of the 12.3 cm HT with three configurations of the magnetic field. The electron temperature profile, $T_{exper}(z)$, quantitatively similar to the one measured with the fast reciprocating emissive probe³⁵ in the same 12.3 cm HT at $V_d = 300\text{V}$ and $\dot{m} = 5\text{mg/s}$ is given in Fig. 6 (a). In Ref. 35, currents in the inner and primary outer coils were kept equal to 1 A and 2.5 A, respectively, and the current in the auxiliary outer coil was equal to zero. It was shown that using a simplified temperature profile, $T_e(z)$, also given in Fig. 6 (a), instead of $T_{exper}(z)$ for modeling of the thruster with B_0 configuration of the magnetic field insignificantly affects modeling results. The electron temperature profile used here for modeling with B_{pos} configuration is given in Fig. 6 (b). Based on the fact that the near-anode electron temperature measured in B_{pos} configuration is higher than that in B_0 configuration, the maximum temperature in B_{pos} configuration is selected to be higher than that in B_0 configuration. In B_{neg} configuration, the maximum temperature is also selected to be higher than that in B_0 configuration, and the location of the maximum is selected to be in the region where the axial component of the magnetic field is predominant [Figs. 6 (c) and 2 (c)], due to the above reasons.

In our quasi 1-D model all vectors are projected onto the z - axis, where z is the coordinate along the thruster axis, with $z = 0$ at the anode. The physical processes in a Hall thruster can be then expressed mathematically as follows:

$$J'_i = \langle \sigma V \rangle n_a n - 0.55 n \sqrt{T_e / M_i} \times 2 / H_{ch} \quad (5.1)$$

is the ion continuity equation. Here, the prime sign denotes the derivative with respect to z , $J_i = n \cdot V_i$ is the ion flux, n is the plasma density, V_i is the ion flow velocity, M_i is the Xenon ion mass, and n_a is the neutral density. The first term in (5.1) represents ionization, and the second term represents wall losses averaged over a channel width. Wall losses are considered zero outside the channel. The ionization coefficient, $\langle \sigma V \rangle (T_e)$, and the factor 0.55 are explained in Ref. 24.

$$(J_i V_i)' = e E n / M_i - 0.55 n \sqrt{T_e / M_i} \times 2 / H_{ch} \times V_i + \langle \sigma V \rangle n_a n \times V_a \quad (5.2)$$

is the ion momentum equation. Here E is the axial projection of the electric field. The first term on the RHS of this equation is the ion acceleration in the electric field. The second and the third terms originate

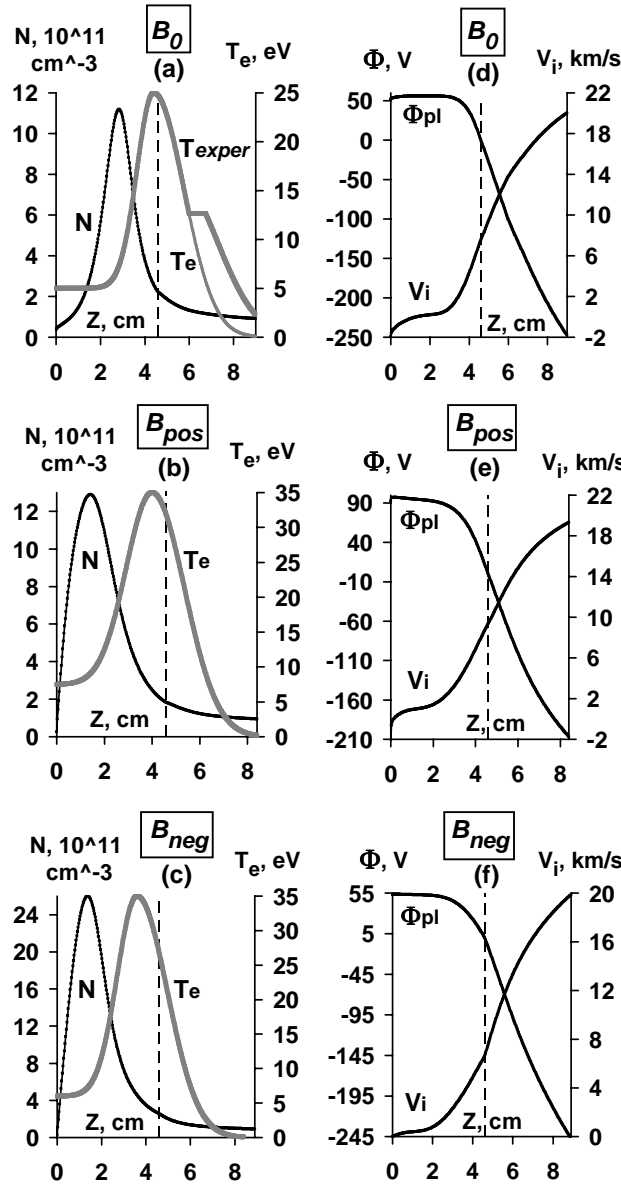


Figure 6: (a) – (c) – electron temperature axial profiles, $T_e(z)$, used in the simulations, and numerically obtained plasma density profiles, $N(z)$, in the 12.3 cm Hall thruster with three magnetic field configurations, B_0 , B_{pos} , and B_{neg} . (d) – (f) – numerically obtained electric potential and ion velocity axial profiles, $\Phi(z)$ and $V_i(z)$. For $V_d = 300$ V and $\dot{m} = 3$ mg/s. All solutions are constructed on the intervals between the anode and the cathode planes, $Z = 0$ and $Z = L_{cath}$, respectively. The vertical dashed lines denote the channel exit, where zero potential is chosen.

from ion losses to the walls with the ion flow velocity, V_i , and ion production with the neutral flow velocity, V_a , respectively.

$$n_a V_{a0} + J_i = J_m \quad (5.3)$$

represents mass conservation. Here $J_m = \dot{m}/(M_i \cdot AA)$ is the propellant flux.

$$-en\mu_e^{-1}V_e = eEn + (n_e T_e)' \quad (5.4)$$

is the phenomenological electron momentum equation, in which μ_e is the absolute value of the electron axial mobility in a radial magnetic field. We assume a modified Bohm diffusion with $\mu_e = \alpha/(16|B_r(z)|)$, where the fitting parameter α is to be determined by the modeling.

$$-nV_e + J_i = J_d \quad (5.5)$$

represents charge conservation. Here, $J_d = I_d/(e \cdot AA)$, and the measured values of the discharge current, I_d , given in Fig. 4 were used for modeling in each configuration of the magnetic field.

The system of equations (5.1) – (5.5) can be reduced to the system of two ordinary differential equations for the plasma density, $n(z)$, and the ion flux, $J_i(z) = n(z)V_i(z)$, of the form:

$$\begin{cases} dJ_i/dz = F(J_i, n, J_d, \alpha) \\ dn/dz = G(J_i, n, J_d, \alpha)/(1 - V_i^2/V_s^2) \end{cases} \quad (5.6)$$

where F and G are nonlinear functions, and $V_s = \sqrt{T_e/M_i}$ is the ion acoustic velocity. In all three configurations of the magnetic field, a solution of the system (5.6) can be constructed, if the ion velocity and the plasma density at the anode, V_{i0} and n_0 , and the electron mobility coefficient, α , are specified. The plasma density measured at 2 mm from the anode in the midpoint between the channel walls [Figs. 5 (a) – (c)] is used in this modeling as n_0 . Based on observations of the electron-repelling anode sheath in B_0 and B_{pos} configurations [Figs. 4 (a) and (b)], a back ion flow with the ion acoustic velocity at the quasineutral plasma boundary is assumed in these configurations to set the boundary condition for the ion velocity: $V_{i0} = -V_s$. In B_{neg} configuration, a zero ion velocity is assumed at $z = 0$: $V_{i0} = 0$. Finally, similar to Ref. 24 it can be shown that for each pair of V_{i0} and n_0 there is only one value of α , for which a solution is regular at the sonic transition point: $V_{i0} = V_s$.

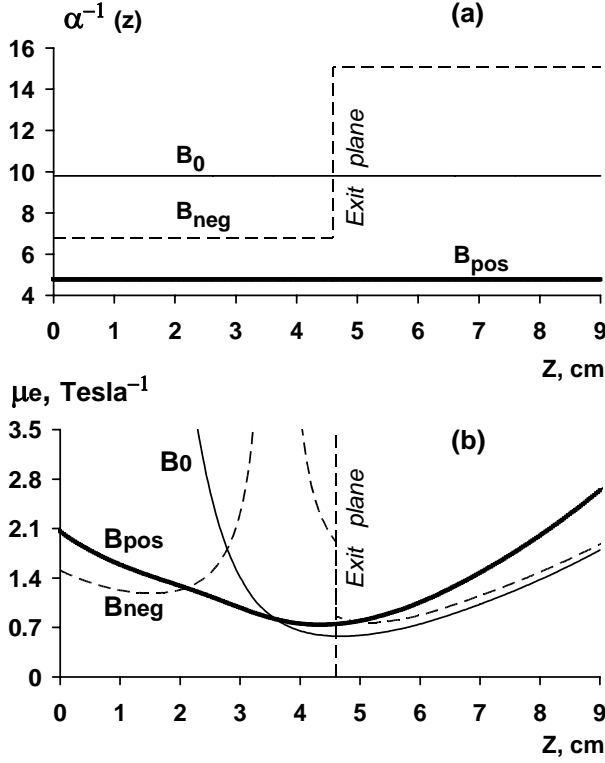


Figure 7: (a) – axial profiles of the reversed electron mobility coefficient, $\alpha^{-1}(z)$, and (b) – the electron axial mobility, $\mu_e(z)$, obtained numerically for the 12.3 cm Hall thruster with three magnetic field configurations, B_0 , B_{pos} , and B_{neg} . For discharge voltage $V_d = 300$ V and mass flow rate $\dot{m} = 3$ mg/s. $Z = 0$ is chosen in the anode plane.

configurations, a different boundary condition for the ion velocity was used at $z = 0$, as it was shown numerically that changing the boundary condition to $V_{i0} = 0$ does not significantly affect the peak density in these configurations. The following analysis can explain why the numerically obtained peak density in B_{neg} configuration is higher than that in B_{pos} configuration (a similar analysis can be used for comparison between B_{neg} and B_0 configurations). Using eq-s (5.1) – (5.5) it can be obtained that

$$N_{\max} \approx (J_d - J_i) / (\mu_e \cdot T_e' / e) - J_i / (T_e' / M_i) \cdot \{2 < \sigma V_e > (J_m - J_i) / V_a - 1.1 V_s / H_{ch}\} \quad (5.8)$$

where $N_{\max} = N(z_{\max})$ is the peak density, and all functions on the right hand side of eq. (6.2) are evaluated at $z = z_{\max}$. In both configurations, the location of the maximum is almost the same, $z_{\max} \approx 1.37$ cm, as well as T_e' at this point. However, the first term on the RHS of eq. (6.2) is greater in B_{neg} configuration, whereas the second term is greater in B_{pos} configuration. The above is due to the following two facts: (1) – as can be seen from Fig. 7 (b), the electron axial mobility at $z = z_{\max}$, $\mu_e(z_{\max})$, is smaller in B_{neg} configuration than it is in B_{pos} configuration, and (2) – the ion flux at $z = z_{\max}$, $J_i(z_{\max})$, is greater in B_{pos} configuration than it is in B_{neg} configuration, which, in turn, is due to the larger near-anode electron temperature in B_{pos} configuration. Thus, within the framework of the presented model, the larger peak density obtained in B_{neg} configuration is due to the smaller near-anode electron temperature and axial mobility in this configuration. The larger peak density and the smaller ion flux at $z = z_{\max}$ also mean that the ion velocity at this location is smaller in B_{neg} configuration than it is in B_{pos} configuration. This fact can be explained from a slightly different perspective. In Ref. 24, the equation determining dM/dz , where

VI. Numerical Results

System (5.6) was integrated numerically in all three configurations of the magnetic field, B_0 , B_{pos} , and B_{neg} . The integration was initiated at the anode, $z = 0$, and terminated at the point in the cathode plane, $z = L_{cath}$, determined by

$$\int_0^{L_{cath}} E(z) dz = V_d \quad (5.7)$$

In B_0 and B_{pos} configurations, the cathode plane was found to be at 8.9 cm and 8.4 cm from the anode, respectively. In B_{neg} configuration, however, it was impossible to select L_{cath} based on the above condition, because for $z \rightarrow \infty$, the electric potential saturated at approximately 250 V below the anode potential, whereas the discharge voltage $V_d = 300$ V. To obtain the voltage drop across the discharge equal to V_d , the electron mobility coefficient, α , outside the channel was allowed to be different from that inside the channel. Thus, in B_{neg} configuration, L_{cath} was selected the same as that in B_0 configuration, and eq. (6.1) was satisfied by selecting an appropriate α outside the channel.

The plasma potential, plasma density, and ion velocity obtained numerically in all three configurations of the magnetic field are given in Fig. 6. As can be seen from Figs. 6 (a) – (c), the peak plasma density obtained in B_{neg} configuration is almost twice as large as it is in B_0 and B_{pos} configurations. This behavior can not be attributed to the fact that in B_0 and B_{pos}

$M = V_i/V_s$, is obtained from the system (5.1) – (5.5). It is shown that in this equation, the term proportional to the ionization rate, $v_i = \langle \sigma V_e \rangle (J_m - J_i)/V_a$, effectively acts as an acceleration force for ions in the subsonic plasma with $V_i > 0$, whereas the term proportional to $(J_d - J_i)/\mu_e$ effectively acts as a drag force. Smaller near-anode electron temperature and axial mobility in B_{neg} configuration (compared to that in B_{pos} configuration) result in the smaller acceleration term and the larger drag term, ultimately leading to the smaller ion velocity at $z = z_{\text{max}}$.

The reversed electron mobility coefficients, α^{-1} , obtained numerically in all three configurations of the magnetic field are given in Fig. 7 (a). These coefficients were used to plot the electron mobility axial profiles, $\mu_e(z)$, given in Fig. 7 (b). Inside the channel, the largest α is found in B_{pos} configuration, and the smallest α is found in B_0 configuration. The numerical solution obtained in B_{neg} configuration suggests that the electron mobility coefficient outside the thruster channel is approximately twice as small as it is inside, and that the most part of the discharge voltage drop occurs outside the channel, where the electron mobility is generally smaller. In the stationary plasma thruster model reported in Ref. 46, different mechanisms of the electron mobility and different mobility coefficients were considered inside and outside the thruster channel. In this model, the most part of the discharge voltage drop was also found to be in the region with smaller electron mobility.

VII. Summary and Conclusions

Effect of the magnetic field profile on the anode fall in a 2 kW laboratory Hall thruster is studied both experimentally and theoretically. Plasma potential, electron temperature, and plasma density in the near-anode region are measured with a biased probe in three configurations of the magnetic field. In varying the magnetic field topology in the channel from a more uniform to a cusp-like one with a zero-field region, we uncover intriguing results. For cusp configurations, in which the radial magnetic field changes polarity somewhere along the channel, the anode fall is positive, whereas it is negative for a more uniform field. This polarity difference could be attributed to the decreased electron mobility across the magnetic field in the cusp-like configuration. Most interesting is that it is the magnetic field topology in the bulk of the discharge, far from the anode, that determines the electron crossed-field mobility and the sign of the anode fall. This new information about the anode sheath in different configurations of the magnetic field now can underpin theoretical modeling in a variety of applications by setting proper boundary conditions at the anode. Different anode sheath regimes observed experimentally were used here to set the boundary conditions for the quasineutral plasma. Numerical solutions obtained with a hydrodynamic quasi-1D model suggest that varying the magnetic configuration affects the electron mobility both inside and outside the channel, as well as the plasma density distribution along the axis. Namely, it was found that in the cusp configuration with a zero-field region: (1) – the electron mobility outside the channel must be assumed almost twice as small as the mobility inside to allow the voltage drop over the discharge be equal to the applied voltage, and (2) – the peak plasma density is almost twice as big as the peak density in the other two configurations studied. Different motilities inside and outside the channel have been discussed in recent theoretical works in conjunction with modeling of the conventional (like SPT-100) and advanced (like ATON) thrusters. In these models, like in our work, the most part of the discharge voltage drop was also found to be in the region with smaller electron mobility.

Acknowledgment

The authors wish to thank A. Smirnov for fruitful discussions. This work was supported by the US DOE under contract No. DE-AC02-76CH03073.

References

1. A. I. Morozov and V. V. Savelyev, “Fundamentals of Stationary Plasma Thruster Theory”, In *Reviews of Plasma Physics*, edited by B. B. Kadomtsev and V. D. Shafranov (Kluwer Academic/Plenum Publishers, New York, 2000), Vol. 21.
2. V. V. Zhurin, H. R. Kaufman, and R. S. Robinson, “Physics of Closed Drift Thrusters”, *Plasma Sources Sci. Technol.* **8**, R1 (1999).
3. R. G. Jahn, “Physics of Electric Propulsion”, (New York, McGraw-Hill Book Company, 1968).

4. H. R. Kaufman, "Ion-Thruster Propellant Utilization", *J. Spacecraft and Rockets* **9**, 511 (1972).
5. R. G. Jahn and E. Y. Choueiri, "Electric Propulsion", In *Encyclopedia of Physical Science and Technology, 3rd Edition* (Academic Press, San Diego), Vol. 5, p. 125. (2002).
6. A. I. Morozov, Yu. V. Esipchuk, A. M. Kapulkin, V. A. Nevrovskii, and V. A. Smirnov, "Effect of the Magnetic Field on a Closed-Electron Drift Accelerator", *Sov. Phys. Tech. Phys.* **17**, 482 (1972).
7. A. I. Morozov, "On equilibrium and stability of flows in accelerators with closed electron drift and extended acceleration zone", In *Plasma Accelerators* (a collection of papers from the *1st All-Union Conference on Plasma Accelerators*), edited by L. A. Artsimovich, S. D. Grishin, G. L. Grodzovsky, L. V. Leskov, A. I. Morozov, A. A. Porotnikov, A. M. Dorodnov, V. G. Padalka, and M. I. Pergament (Mashinostroenie, Moscow, 1973), p. 85 (Rus.).
8. A. I. Morozov and V. V. Savelyev. In *Reviews of Plasma Physics*, edited by B. B. Kadomtsev and V. D. Shafranov (Kluwer Academic/Plenum Publishers, New York, 2000), Vol. 21. p. 351.
9. A. I. Morozov, Yu. V. Esinchuk, G. N. Tilinin, A. V. Trofimov, Yu. A. Sharov, and G. Ya. Shchepkin, "Plasma Accelerator with Closed Electron Drift and Extended Acceleration Zone", *Sov. Phys. Tech. Phys.* **17**, 38 (1972).
10. I. V. Melikov, "Experimental Investigation of Anode Processes in a Closed electron-drift accelerator", *Sov. Phys. Tech. Phys.* **19**, 35 (1974).
11. I. V. Melikov, "Point and Jet Ionization in a Hall Plasma Accelerator", *Sov. Phys. Tech. Phys.* **22**, 452 (1977).
12. A. M. Bishaev and V. Kim, "Local Plasma Properties in a Hall-Current Accelerator with an Extended Acceleration Zone", *Sov. Phys. Tech. Phys.* **23**, 1055 (1978).
13. G. Guerrini, C. Michaut, M. Bacal, A. N. Vesselovzorov, and A. A. Pogorelov, "An intense Hall-type ion source for satellite propulsion", *Rev. Sci. Instrum.* **69**, 804 (1998). See also: G. Guerrini, C. Michaut, M. Dudeck, A. N. Vesselovzorov, and M. Bacal, "Characterization of Plasma Inside the SPT-50 Channel by Electrostatic Probes", Proceedings of the *25th International Electric Propulsion Conference*, Aug 1997, Cleveland, OH, IEPC Paper 1997-053.
14. Y. Raitses, J. Ashkenazy and M. Guelman, "Propellant Utilization in Hall Thrusters", *J. Prop. Power* **14**, 247 (1998).
15. Y. Raitses, L. A. Dorf, A. A. Litvak, and N. J. Fisch, "Plume Reduction in Segmented Electrode Hall Thruster", *J. Appl. Phys.* **88**, 1263 (2000).
16. N. J. Fisch, Y. Raitses, L. A. Dorf, and A. A. Litvak, "Variable Operation of Hall Thruster with Multiple Segmented Electrodes", *J. Appl. Phys.* **89**, 2040 (2001).
17. Y. Raitses, M. Keidar, D. Staack, N. J. Fisch, "Effects of Segmented Electrode in Hall Current Plasma Thruster", *J. Appl. Phys.* **92**, 4906 (2002).
18. J. M. Haas and A. D. Gallimore, "Internal Plasma Potential Profiles in a Laboratory-Model Hall Thruster", *Phys. Plasmas* **8**, 652 (2001).
19. N. B. Meezan, W. A. Hargus, Jr. and M. A. Cappelli, "Anomalous Electron Mobility in a Coaxial Hall Discharge Plasma", *Phys. Rev. E* **63**, Art. No. 026410 (2001).
20. N. Z. Warner, J. J. Szabo and M. Martinez-Sanchez, "Characterization of a High Specific Impulse Hall Thruster Using Electrostatic Probes", Proceedings of the *28th International Electric Propulsion Conference*, March 2003, Toulouse, France, IEPC Paper 2003-082.
21. E. Ahedo, P. Martinez-Cerezo, M. Martinez-Sanchez, "One-Dimensional Model of a Plasma Flow in a Hall Thruster", *Phys. Plasmas* **8**, 3058 (2001).
22. A. Fruchtman, N. J. Fisch, and Y. Raitses., "Control of the Electric Field Profile in the Hall Thruster", *Phys. Plasmas* **8**, 1048 (2001).
23. M. Keidar, I. Boyd and I. Beilis, "Analyses of the Anode Region in a Hall Thruster Channel", Proceedings of the *38th Joint Propulsion Conference and Exhibit*, July 2002, Indianapolis, IN, AIAA Paper 2002-4107.
24. L. Dorf, V. Semenov, Y. Raitses, and N. J. Fisch, "Hall Thruster Modeling with a Given Temperature Profile", Proceedings of the *38th Joint Propulsion Conference and Exhibit*, July 2002, Indianapolis, Indiana, AIAA Paper 2002-4246.
25. L. Dorf, Y. Raitses, V. Semenov, and N. J. Fisch, "Effect of Anode Dielectric Coating on Hall Thruster Operation", *Appl. Phys. Lett.* **84**, 1070 (2004).
26. L. Dorf, Y. Raitses, and N. J. Fisch, "Experimental studies of anode sheath phenomena in a Hall thruster discharge", *J. Appl. Phys.* **97**, 103309 (2005). See also: L. Dorf, *Studies of Anode Sheath Phenomena in Hall Thrusters*. Ph.D. Dissertation. Princeton University, Princeton, NJ 08544, USA (2004).
27. L. Dorf, Y. Raitses, and N. J. Fisch, "Electrostatic Probe Apparatus for Measurements in the Near-Anode Region of Hall Thruster", *Rev. Sci. Instrum.*, **75**, 1255 (2004).
28. L. Dorf, V. Semenov, and Y. Raitses, "Anode Sheath in Hall Thrusters", *Appl. Phys. Lett.* **83**, 2551 (2003).

29. J. E. Foster and A. D. Gallimore, "An Investigation into the Role that a Transverse Magnetic Field Plays in the Formation of Large Anode Sheath Potentials", *Phys. Plasmas* **3**, 4239 (1996).
30. N. A. Kervalishvili, V. P. Kortkhondzhiya, and G. B. Machabeli, "Electron Motion and Structure of the Anode Sheath with a Deviation from $E \perp B$ in a Low-Pressure Discharge", *Sov. Phys. Tech. Phys.* **20**, 512 (1975).
31. E. V. Shun'ko, "Influence of a Magnetic Field Parallel to the Cathode Surface on the Near-Cathode Drop in the Potential in a Normal Glow Discharge", *Phys. Letters A* **128**, 433 (1988).
32. L. Pekker, "Longitudinal Distribution of Plasma Density in the Low-Pressure Glow Discharge with Transverse Magnetic Field", *Plasma Sources Sci. Technol.* **4**, 31 (1995).
33. M. A. Hassouba, "Effect of the Magnetic Field on the Plasma Parameters in the Cathode Fall Region of the Dc-Glow Discharge", *Eur. Phys. J. AP* **14**, 131 (2001).
34. K. Wasa and S. Hayakawa, "Handbook of Sputter Deposition Technology: Principles, Technology, and Applications" (Noyes, Park Ridge, 1992).
35. Y. Raitses, D. Staack, A. Smirnov, and N. J. Fisch, "Space charge saturated sheath regime and electron temperature saturation in Hall thrusters", *Phys. Plasmas* **12**, 073507 (2005). See also: Y. Raitses, D. Staack, L. Dorf and N. J. Fisch, "Experimental Study of Acceleration Region in a 2 kW Hall Thruster", Proceedings of the 39th Joint Propulsion Conference and Exhibit, July 2003, Huntsville, AL, AIAA Paper 2003-5153.
36. Y. M. Kagan, V. I. Perel, "Plasma Diagnostics in a Magnetic Field Using Thin Cylindrical Probes", *Sov. Phys. Tech. Phys.* **13**, 1348 (1969).
37. A. Smirnov, Y. Raitses, and N. J. Fisch, "Electron cross-field transport in a low power cylindrical Hall thruster", *Phys. Plasmas* **11**, 4922 (2004).
38. M. Keidar, I. D. Boyd, and I. I. Beilis, "Plasma Flow and Plasma-Wall Transition in Hall Thruster Channel", *Phys. Plasmas* **8**, 5315 (2001).
39. A. Smirnov, Y. Raitses, and N. J. Fisch, "Parametric investigation of miniaturized cylindrical and annular Hall thrusters", *J. Appl. Phys.* **92**, 5673 (2002).
40. L. Garrigues, G. J. M. Hagelaar, J. Bareilles, C. Boniface, and J. P. Boeuf, "Model study of the influence of the magnetic field configuration on the performance and lifetime of a Hall thruster", *Phys. Plasmas* **10**, 4886 (2003).
41. M. Touzeau, M. Prioul, S. Roche, N. Gascon, C. Pe´rot, F. Darnon, S. Be´chu, C. Philippe-Kadlec, L. Magne, P. Lasgorceix, D. Pagnon, A. Bouchoule, and M. Dudeck, "Plasma diagnostic systems for Hall-effect plasma thrusters", *Plasma Phys. Controlled Fusion* **42**, B323 (2000).
42. A. I. Morozov, A. I. Bugrova, A. V. Desyatskov, Yu. A. Ermakov, M. V. Kozintseva, A. S. Lipatov, A. A. Pushkin, V. K. Khartchevnikov, and D. V. Churbanov, "ATON-Thruster Plasma Accelerator", *Plasma Phys. Rep.* **23**, 587 (1997).
43. V. S. Golubev, Yu. N. Krivenko, P. G. Leonov, and V. B. Flerov, "Coaxial laser with magnetic discharge stabilization", *Sov. Tech. Phys. Lett.* **14**, 662 (1988).
44. A. I. Bugrova, L. M. Volkova, V. A. Ermolenko, E. A. Kral'kina, A. M. Devyatov, and V. K. Kharchevnikov, "Dynamics of the Electron Energy Distribution Function in a Plasma Accelerator with Extended Acceleration Zone", *High Temp.* **19**, 822 (1981).
45. V. Yu. Fedotov, A. A. Ivanov, G. Guerrini, A. N. Vesselovzorov, and M. Bacal, "On the electron energy distribution function in a Hall-type thruster", *Phys. plasmas* **6**, 4360 (1999).
46. G. J. M. Hagelaar, J. Bareilles, L. Carrigues, and J.-P. Boeuf, "Role of Anomalous Electron Transport in a Stationary Plasma Thruster Simulation", *J. Appl. Phys.* **93**, 67 (2003).